Journal of Cerebral Blood Flow & Metabolism (2012) 32, 1919–1932

www.jcbfm.com

Increased intracranial pressure after diffuse traumatic brain injury exacerbates neuronal somatic membrane poration but not axonal injury: evidence for primary intracranial pressure-induced neuronal perturbation

Audrey D Lafrenaye, Melissa J McGinn and John T Povlishock

Department of Anatomy and Neurobiology, Virginia Commonwealth University Medical Center, Richmond, Virginia, USA

Increased intracranial pressure (ICP) associated with traumatic brain injury (TBI) is linked to increased morbidity. Although our understanding of the pathobiology of TBI has expanded, questions remain regarding the specific neuronal somatic and axonal damaging consequences of elevated ICP, independent of its impact on cerebral perfusion pressure (CPP). To investigate this, Fischer rats were subjected to moderate TBI. Measurements of ICP revealed two distinct responses to injury. One population exhibited transient increases in ICP that returned to baseline levels acutely, while the other displayed persistent ICP elevation (>20 mm Hg). Utilizing these populations, the effect of elevated ICP on neuronal pathology associated with diffuse TBI was analyzed at 6 hours after TBI. No difference in axonal injury was observed, however, rats exhibiting persistently elevated ICP postinjury revealed a doubling of neurons with chronic membrane poration compared with rats exhibiting only transient increases in ICP. Elevated postinjury ICP was not associated with a concurrent increase in DNA damage; however, traditional histological assessments did reveal increased neuronal damage, potentially associated with redistribution of cathepsin-B from the lysosomal compartment into the cytosol. These findings indicate that persistently increased ICP, without deleterious alteration of CPP, exacerbates neuronal plasmalemmal perturbation that could precipitate persistent neuronal impairment and ultimate neuronal death.
Journal of Cerebral Blood Flow & Metabolism (2012) **32,** 1919–1932; doi:10.1038/jcbfm.2012.95; published online 11 July 2012

Keywords: animal models; basic science; brain trauma; cathepsin-B; intracranial pressure; membrane poration

Introduction

Diffuse traumatic brain injury (TBI) is a major health concern with devastating personal and societal consequences (Langlois *et al*, 2006). Although our understanding of TBI has improved with an enhanced appreciation of injury-induced neuronal pathology and axonal perturbation, currently little insight exists into the complex pathobiology of neurons sustaining mechanical/TBI-induced membrane poration. Previously, our laboratory has shown that neurons in the lateral neocortex show mechanoporation after diffuse TBI and that a subset of these mechanoporated neurons progress to necrotic change (Singleton and Povlishock, 2004; Farkas *et al*, 2006). These findings have been corroborated *in vitro* by the demonstration of membrane poration and ultimate neuronal death after mechanical injury (Geddes *et al*, 2003*b*; LaPlaca *et al*, 2009; Cullen *et al*, 2011), thereby reaffirming the importance of this membrane poration. Paralleling membrane perturbation is the occurrence of traumatically induced diffuse axonal injury; a pathology that contributes to posttraumatic morbidity and may be related to focal axolemmal mechanoporation (Singleton and Povlishock, 2004).

Adding to the complexity of mechanically/TBI-induced neuronal somatic mechanoporation and axonal injury is their potential modification by posttraumatic elevations of intracranial pressure (ICP). While this issue has been relatively unexplored in the context of somatic membrane poration or axonal injury, increased ICP after TBI is highly correlated to

Correspondence: Dr JT Povlishock, Department of Anatomy and Neurobiology, Virginia Commonwealth University Medical Center, P.O. Box 980709, Richmond, VA 23298, USA.
E-mail: jtpovlis@vcu.edu
This study is supported by NIH grants NS 045824 and NS 047463.
Received 19 January 2012; revised 19 April 2012; accepted 18 May 2012; published online 11 July 2012

increased long-term morbidity and mortality (Miller *et al*, 1977; Treggiari *et al*, 2007). In fact, the Brain Trauma Foundation recommends that all patients at risk for intracranial hypertension receive ICP monitoring with therapeutic maintenance <20 mm Hg (Bratton *et al*, 2007*b*; http://www.braintrauma.org/coma-guidelines/). However, less than half of the hospitals in the United States are in compliance with these recommendations (Hesdorffer *et al*, 2002).

To date, the majority of research on increased ICP after TBI has focused on the potential for elevated ICP to alter cerebral perfusion pressure (CPP) to the point of eliciting ischemia (Li *et al*, 2010); however, other important questions remain regarding the specific damaging consequences of elevated ICP independent of its impact on CPP. Therefore, the current study examined the effects of increased ICP on the magnitude of TBI-induced somatic membrane perturbation/poration as well as the overall burden of axonal damage.

To this end, we used a central fluid percussion injury (CFPI) model of TBI (Dixon *et al*, 1987) on adult Fischer rats, which show acute ICP sensitivity to TBI (Reid *et al*, 2010). Interestingly, we observed two patterns of ICP after injury, one in which ICP increased >20 mm Hg returning to baseline levels acutely and a second pattern which maintained persistently elevated ICP >20 mm Hg. The burden of axonal injury was comparable between these two ICP groups; however, the number of both histologically damaged and chronically mechanoporated neurons increased in the lateral neocortex of animals with persistently elevated ICP compared with animals with transient ICP elevation after injury. These chronically porated neurons underwent necrotic change and showed a redistribution of cathepsin-B from the lysosomal compartment to the cytosol, pointing toward a neuronal pathology that appears to transition to cell death.

Materials and methods

General Preparation

Experiments were conducted using protocols in accordance with the Virginia Commonwealth University institutional guidelines concerning the care and use of laboratory animals (Institutional Animal Care and Use Committee, Virginia Commonwealth University). Animals were housed in individual cages on a 12 hours light–dark cycle, with free access to food and water.

Animal Numbers

In all, 45 adult male Fischer rats weighing 295 to 345 g were used. Five animals were used as sham-injured controls. Fifty-six percent of the injured animals were excluded from analysis because of failure to meet the rigorous physiological inclusion criteria as detailed below. Due to the large percentage of animals excluded, the fewest possible animals required to reach statistical significance were used. A two-tailed, two-sample power analysis, using averages and standard deviations of the sham-injured, low ICP and high ICP group's membrane poration data, comparing each group with each other group, was performed to verify appropriate animal numbers. The power was $>85\%$ with a confidence interval of 95%.

Surgical Preparation and Injury Induction

Animals were intubated and ventilated with 1% to 1.5% isoflurane, 30% O_2, and 70% N_2O throughout the duration of the experiment until euthanasia and transcardial perfusion at 6 hours after injury. Animals were placed on a feedback-controlled heating pad (Harvard Apparatus, Holliston, MA, USA) to maintain body temperature at 37°C. A PE50 polyethylene tube connected to a closed pressure system (Becton Dickinson, Sparks, MD, USA) was placed into the right femoral artery to monitor the mean arterial blood pressure (MABP). After cannulation, animals were placed in a stereotaxic frame (David Kopf Instruments, Tujunga, CA, USA). A midline incision was made between bregma and lambda and a 4.8-mm circular craniotomy was made along the sagittal suture midway between bregma and lambda for injury induction. A 2-mm burr hole was also drilled into the left parietal bone overlying the left lateral ventricle (0.8 mm posterior, 1.3 mm lateral, and 2.5 to 3 mm ventral relative to bregma) through which a 25-gauge needle, connected to a pressure transducer and a microinfusion Pump 11 Elite syringe pump (Harvard Apparatus) via PE50 tubing, was placed into the ventricle. Appropriate placement was verified via a 3-μL/min infusion of sterile saline within the closed fluid-pressure system during needle placement (Sullivan *et al*, 1976). Ten minutes after needle placement, 15 μL of Alexa Fluor 568-conjugated or Alexa Fluor 488-conjugated 10 kDa dextran (40 mg/mL in sterile 0.9% saline; 2 mg/kg; Invitrogen, San Diego, CA, USA) was infused into the left lateral ventricle at 1 to 2 μL/min, with continuous ICP monitoring. The needle remained in the ventricle for 20 minutes after completion of the tracer infusion and then was slowly removed. Bone wax was used to seal the burr hole used for dextran infusion before preparation for CFPI. The procedures by which rats were subjected to CFPI were consistent with those described previously (Dixon *et al*, 1987; Singleton and Povlishock, 2004). Briefly, a Leur-Loc syringe hub was affixed to the craniotomy site and dental acrylic (methyl-methacrylate; Hygenic Corp., Akron, OH, USA) was applied around the hub, including the area overlying the sealed burr hole and allowed to harden. Forty-five minutes after the completion of the preinjury dextran infusion, the animal was injured at a magnitude of 1.86 ± 0.4 atmospheres. The pressure pulse measured by the transducer was displayed on an oscilloscope (Tektronix, Beaverton, OR, USA). Immediately after the injury, the animal was reconnected to the ventilator and all physiological monitoring devices. The hub, dental acrylic, and bone wax were removed en bloc and Gel foam was placed over the craniotomy/injury site. The animal was replaced in the stereotaxic device and ICP monitoring

was resumed as described above. Identical surgical procedures were followed for sham-injured control animals, without the release of the pendulum to induce the injury.

Delayed Tracer Infusion

A second tracer infusion was performed from 4.5 to 5 hours after injury. The ICP needle was reinserted into the lateral ventricle and Alexa Fluor 568-conjugated or Alexa Fluor 488-conjugated 10 kDa dextran was infused in the same manner as the preinjury dextran at a rate of 0.5 to 1 μL/min, with continuous ICP monitoring. The tracer was allowed to diffuse for an additional hour before transcardial perfusion.

Physiological Assessment

Physiological monitoring was performed throughout the duration of the experiment, except during the induction of injury. The femoral artery was cannulated for MABP monitoring and blood gas analysis (Stat Profile pHOx, Nova Biomedical, Waltham, MA, USA). Blood gas analysis was performed at the completion of the experiment to confirm the ongoing physiological measurements. The ICP was measured intraventricularly as described above. Heart rate, respiratory rate, and blood oxygenation were monitored via a foot pulse oximetry sensor (STARR Life Sciences, Oakmont, PA, USA). A PowerLab system (AD Instruments, Colorado Springs, CO, USA) was used to record all physiological parameters (MABP, ICP, heart rate, and blood oxygenation) throughout the duration of the experiment. The CPP was determined by subtracting the ICP from the MABP. Any animal failing to meet the physiological inclusion criteria set forth for the study (i.e., MABP >60 mm Hg, CPP >50 mm Hg, oxygenation $>90\%$, heart rate >200 BPM) was excluded from analysis.

Tissue Processing

At 6 hours after TBI, the animals were injected with 150 mg/kg euthasol and then underwent transcardial perfusion with 0.9% saline followed by 4% paraformaldehyde in Millonig's buffer (136 mmol/L sodium phosphate monobasic/109 mmol/L sodium hydroxide) for immunohistochemical analysis or 4% paraformaldehyde/0.2% glutaraldehyde in Millonig's buffer for electron microscopic processing. After transcardial perfusion, the brains were removed, postfixed for 24 hours, and then sectioned coronally in 0.1 mol/L phosphate buffer with a vibratome (Leica, Banockburn, IL, USA) at a thickness of 40 μm from bregma to $\sim$4.0 mm posterior to bregma. Sections were collected serially in 12-well plates and stored in Millonig's buffer at 4°C.

Fluorescent Immunohistochemistry

Because the infused dextran tracers were conjugated to fluorophores (Alexa Fluor 488 and Alexa Fluor 568), no additional steps were required for confocal microscopic visualization of any dextran-containing cells. In addition to the identification of the dextran tracer, a mouse antibody against NeuN (Cat. #MAB377, 1:500; Millipore, Billerica, MA, USA) was used to identify neurons, a rabbit antibody against cleaved caspase-3 (Cat. #9661, 1:1,000; Cell Signaling, Danvers, MA, USA) was used to identify apoptotic cells, and a rabbit antibody against cathepsin-B (Cat. #06-480, 1:200; Millipore) was used to analyze cathepsin-B localization. In this procedure, sections were blocked with 10% normal goat serum, permeabilized with 1.5% Triton in normal goat serum, and immunolabeled with the above primary antibodies. Secondary antibodies Alexa Fluor 633-conjugated goat anti-mouse IgG and Alexa Fluor 633-conjugated goat anti-rabbit IgG (Cat. # A21052 and A21071, 1:250; Invitrogen) were then incubated and the tissue was mounted with Vectashield hardset mounting medium with Dapi (Cat. #H-1500; Vector Laboratories, Burlingame, CA, USA). To visualize DNA fragmentation within degenerating cells an ApopTag apoptosis detection kit (Millipore) was used in accordance with manufacturer's recommendations through incubation with the stop/wash buffer after the TdT enzyme reaction. After cessation of the enzymatic reaction, tissue was incubated in mouse anti-Digoxigenin primary antibody (Cat. #11 333 062 910, 1:250; Roche, Basel, Switzerland). Then, Alexa Fluor 633-conjugated goat anti-mouse IgG secondary antibody was used and the tissue was mounted. Sections were analyzed by confocal microscopy using a Leica TCS SP2 AOBS System (Leica).

Electron Microscopy

Because the used fluorescent dye tracers are not detectable at the electron microscopic level, for parallel assessments of the ultrastructural change, the tissue was immunolabeled with antibodies targeting Alexa Fluor 488, which was conjugated to the dextran infused at 4 hours after injury, as described previously (Farkas *et al*, 2006). This method allowed for the ultrastructural assessment of any alteration associated with enduring or delayed membrane change. Briefly, the tissue was immunolabeled with the following antibodies: rabbit anti-Alexa Fluor 488 (Cat. #A-11094, 1:5,000; Invitrogen), rabbit anti-cathepsin-B and secondary antibody biotinylated anti-rabbit IgG (1:1,000; Vector Laboratories). The reaction product was visualized with 0.05% diaminobenzidine/0.01% hydrogen peroxide/0.3% imidazole in 0.1 mol/L phosphate buffer. After the conversion of the Alexa Fluor 488-conjugated dextran, tissue was prepared for electron microscopic analysis. In this approach, regions of interest were dissected from the tissue sections and osmicated, dehydrated, and embedded in epoxy resin on plastic slides. After resin curing, the slides were studied with routine light microscopy to identify the precise neurons of interest. Once identified, these sites were removed, mounted on plastic studs, and 70 nm sections were cut serially and mounted on Formvar-coated slotted grids. The grids were stained in 5% uranyl acetate in 50% methanol and 0.5% lead citrate. Ultrastructural analysis was performed using a JEOL JEM 1230 transmission electron microscope (JEOL-USA,

Peabody, MA, USA) equipped with an Ultrascan 4000 CCD camera (Gatan, Pleasanton, CA, USA).

Detection and Quantification of Axonal Injury

Quantitative analysis was performed in a blinded manner on coronal sections corresponding to 1.8 ± 0.2 mm to 3.8 ± 0.2 mm posterior to bregma (at least 1 mm posterior to the needle track used for ICP monitoring). A random starting well was selected (wells 1 to 12) and four serial sections, each 480 μm apart, were selected for amyloid precursor protein (APP) immunolabeling using a protocol adapted in our laboratory (Stone *et al*, 2000). Briefly, sections were immunolabeled with a primary rabbit antibody against the C terminus of β-APP (Cat. #51-2700, 1:1,000; Invitrogen) followed by secondary antibody biotinylated goat anti-rabbit IgG (Cat. #BA-1000, 1:1,000; Vector Laboratories). The sections were then incubated in avidin biotinylated enzyme complex using the Vectastain ABC kit (Vector Laboratories) followed by visualization with 0.05% diaminobenzidene/0.01% H_2O_2/0.3% imidazole/phosphate-buffered saline. The tissue was mounted, serially dehydrated, and coverslipped with Permount (Cat. #SP15-100; Thermo Fischer Scientific, Waltham, MA, USA). Visualization of APP-labeled axonal swellings was performed using a Nikon Eclipse 800 microscope (Nikon, Tokyo, Japan) equipped with an Olympus DP71 camera (Olympus, Center Valley, PA, USA). Consistent regions of both the left and right neocortex lateral to the hippocampus were imaged at $\times 5$ magnification ($n = 8$ images per animal). Image acquisition settings were held constant for all groups analyzed. Analysis of the number of APP+ axonal swellings was restricted to a $3.75\,\text{mm} \times 1.55\,\text{mm}$ rectangular region encompassing layers V and VI of the lateral neocortex and was performed using the particle analysis function in the ImageJ software (NIH, Bethesda, MD, USA; particle size $> 80\,\mu\text{m}^2$). The number of APP+ swellings per unit area was quantified for each image and averaged for each animal.

Quantification of Neuronal Membrane Perturbation

Quantitative analysis was performed as described above. To reduce variability due to differences in dextran diffusion between the right and left hemispheres, quantification was restricted to dextran-containing neurons within layers V and VI of the left lateral neocortex extending from the area lateral to CA1 to the area lateral to CA3. Confocal images were taken at $\times 40$ magnification within the restricted region of analysis being careful not to duplicate X and Y coordinates ($n = 37$ images per animal; X, Y, and Z coordinates determined by a blinded investigator using Dapi labeling to verify focus). Image acquisition settings were held constant for comparable regions (layer V or VI) for all groups analyzed. Analysis of neurons exhibiting preinjury dextran uptake, postinjury dextran uptake or both preinjury and postinjury dextran uptake was performed using ImageJ software and traditional cell counting. To identify the population of neurons containing both preinjury and postinjury dextran tracers as well as the number of NeuN+ neurons that contained either preinjury or postinjury administered dextrans, the Colocalization Finder plug-in was used and only neurons that contained pixels having an Overlap coefficient of at least 0.9 were included. Dextran-containing neurons were quantified for each image and averaged for each animal.

Hematoxylin and Eosin Analysis and Quantification

To visualize damaged neurons, 40 μm vibratome sections (as described above) were stained with hematoxylin and eosin (H&E). Tissue was mounted onto gelatin-coated slides before dehydration and rehydration. Rehydrated tissue was incubated in hematoxylin followed by washes in ammonia water and a quick dip in eosin before clearing of the sections through increasing concentrations of ethanol. Sections were visualized using a Nikon Eclipse 800 microscope (Nikon) equipped with an Olympus DP71 camera (Olympus). Consistent regions of both the left and right neocortex lateral to the hippocampus were imaged and analyzed by a blinded investigator. Any cell that showed eosinophilic cytoplasm or a condensed nucleus with H&E staining was determined to be damaged.

Quantification of Cathepsin-B Localization

Image acquisition and identification of neurons showing dextran uptake were accomplished as described above. The soma of neurons showing uptake of the preinjury dextran alone, postinjury dextran alone, both dextrans, or no dextran uptake were encircled ($n = 1{,}419$ total neurons; $n = 212$ resealing neurons; $n = 359$ enduring membrane porated neurons; $n = 147$ delayed opening neurons; $n = 701$ nonmechanoporated neurons) and the localization (either punctate or diffuse) of cathepsin-B was noted for each neuron using ImageJ software. The localization of Cathepsin-B was expressed as a percentage of the total neurons for each category having that localization.

For parallel assessment of cathepsin-B localization at the ultrastructural level, immunoelectron microscopy for cathepsin-B was performed on sections in which mechanoporated neurons had already been identified. Briefly, after visualization of the fluorescently labeled mechanoporated neurons, as described above, the sections were soaked off the slides and the tissue was then processed for electron microscopic analysis, as described above. This approach allowed for the analysis of the same neuron at both the fluorescent and ultrastructural levels.

Statistical Analysis

Quantitative data are presented as mean ± s.e.m. For all analysis, an independent group analysis of variance and Fisher LSD *post hoc* analysis were performed; a P value of < 0.05 was considered statistically significant.

Results

Gross Pathological Observations

Moderate CFPI (1.86 ± 0.4 atmospheres), as identified by mortality rates and histological analysis (Dixon *et al*, 1987), generated little gross parenchymal brain alteration. Although the meninges demonstrated hemorrhage, the underlying cortex revealed no sign of contusion, hematoma formation, or tissue loss. No overt cortical compression was observed, although ventricular dilation was common in injured animals regardless of postinjury ICP. The brain parenchyma showed isolated petechial hemorrhages in the subcortical white matter underlying the craniotomy site that did not interfere with neocortical analysis.

Physiological Assessment Revealed Two Injury-Induced Patterns of Intracranial Pressure Elevation

Heart rate, blood oxygenation, and rectal temperature were monitored for the duration of the experiment, both before the induction of injury and for 6 hours after sham or CFPI. Systemic parameters were comparable across experimental groups (data not shown).

The ICP and MABP were also measured throughout the experiment to examine ICP and CPP changes related to moderate diffuse TBI in Fischer rats. No significant elevation in ICP was found in sham-injured animals on either preinjury or postinjury dextran infusion, indicating that the intraventricular infusion itself did not increase ICP ($n = 5$; black bars; Figure 1A). Injured animals, however, did display a modest increase in ICP during the postinjury dextran infusion (Figure 1A).

After CFPI, two patterns of ICP elevation emerged (Figure 1A). Half of the injured animals revealed a transient increase in ICP > 20 mm Hg after injury that returned to baseline levels acutely ($n = 4$; white bars; Figure 1A). The ICP in these animals remained < 20 mm Hg for the majority of the experiment ($> 65\%$ of the 6 hours after injury analysis); accordingly, these injured animals were categorized as the 'low ICP' group. The other half of the injured animals maintained an ICP persistently elevated > 20 mm Hg for the majority of the 6-hour period postinjury and were thus defined as the 'high ICP' group ($n = 5$; gray bars; Figure 1A). If at any point during the experiment the CPP or MABP decreased below normal autoregulatory limits (CPP < 50 mm Hg and MABP < 60 mm Hg; (Bratton *et al*, 2007*a* (http://www.braintrauma.org/coma-guidelines/); Dennis *et al*, 2009; Navarro *et al*, 2012); dashed lines Figures 1B and 1C), then the animal was excluded from analysis. Note that throughout the majority of the experiment the MABP of animals sustaining injury, irrespective of the pattern of postinjury ICP, was comparable to the sham-injured group (Figure 1B). Therefore, the differences in CPP in the high ICP group as compared with either the low ICP or sham groups were primarily due to alterations in postinjury ICP (Figure 1C). There were also no differences in animal weight, age, injury intensity, heart rate, or blood oxygenation between the high and low ICP groups (data not shown) showing that the main difference between these groups was the pattern of ICP after injury, making these naturally emerging groups ideal for analyzing the effect of ICP > 20 mm Hg after diffuse TBI on neuronal pathology.

The Burden of Axonal Injury Is Not Affected by High Intracranial Pressure after Traumatic Brain Injury

As axotomy is a common means of evaluating the magnitude of injury sustained after TBI (Sherriff *et al*, 1994) the effect of persistently elevated ICP on the number of axotomized APP-containing axonal swellings was analyzed. Consistent with previous studies examining axonal injury via APP accumulation, no APP+ swellings were observed in sham-injured animals while diffuse axonal injury was readily apparent in layers V and VI of the lateral neocortex of animals sustaining CFPI (Figure 2). There was no significant difference in the number APP+ swellings in layers V and VI of the lateral neocortex between animals maintaining low ICP after injury (49.09 ± 9.5 swellings) and animals with persistently high ICP postinjury (35.67 ± 4.85 swellings; Figure 2A). This datum suggests that elevated ICP after injury does not affect axonal pathological events that are initiated at the onset of injury as well as substantiates consistency of the injury magnitude for all injured animals.

Persistently High Injury-Induced Intracranial Pressure Is Associated with a Shift in the Population of Membrane Porated Neurons Away from a Resealing Phenotype and Toward Delayed Opening

Based on our previous observation that fluorescently labeled 10 kDa dextrans, normally excluded from the soma by intact membranes, are a reliable way to detect neuronal plasmalemmal alterations (Singleton and Povlishock, 2004; Farkas *et al*, 2006), dextrans conjugated to Alexa Fluor 568 or Alexa Fluor 488 were infused intraventricularly 1.5 to 1 hours before and 4.5 to 5 hours after injury. As previously shown, the administration of fluorescently conjugated dextrans preinjury and at time points postinjury allowed for the visualization of membrane resealing (neurons containing only the preinjury dextran), delayed membrane perturbation (neurons containing only the postinjury dextran), and enduring membrane poration (neurons containing both fluorophores) within the population of membrane-perturbed neurons (Farkas *et al*, 2006).

To determine if high ICP after TBI was associated with a shift in the population of dextran-flooded neurons, an analysis of membrane resealing, delayed membrane perturbation, and enduring membrane

poration was performed. Resealing, enduring, and delayed membrane porated neurons were observed in all injured animals regardless of the postinjury pattern of ICP elevation (Figure 3). The percentage of membrane-perturbed neurons that showed enduring mechanoporation was equivalent in animals maintaining either low ICP ($24.13 \pm 1.42\%$) or high ICP ($26.19 \pm 0.85\%$) after injury. The population of membrane porated neurons that showed membrane resealing was significantly decreased with high ICP after injury (low ICP = $45.52 \pm 3.45\%$; high ICP = $34.63 \pm 1.03\%$ per total porated neurons; $P < 0.05$) while the population of membrane porated neurons that showed delayed membrane perturbation was significantly increased with high ICP after injury (low ICP = $28.32 \pm 3.39\%$; high ICP = $39.18 \pm 1.39\%$ per total porated neurons; $P < 0.05$). This shift of the membrane disrupted population away from resealing and toward delayed membrane perturbation in the high ICP group could be due to one of two phenomena: (1) a decrease in the number of neurons that are initially membrane perturbed after injury or (2) an increase in the number of neurons that are porated more chronically postinjury. Accordingly, these two populations were quantified.

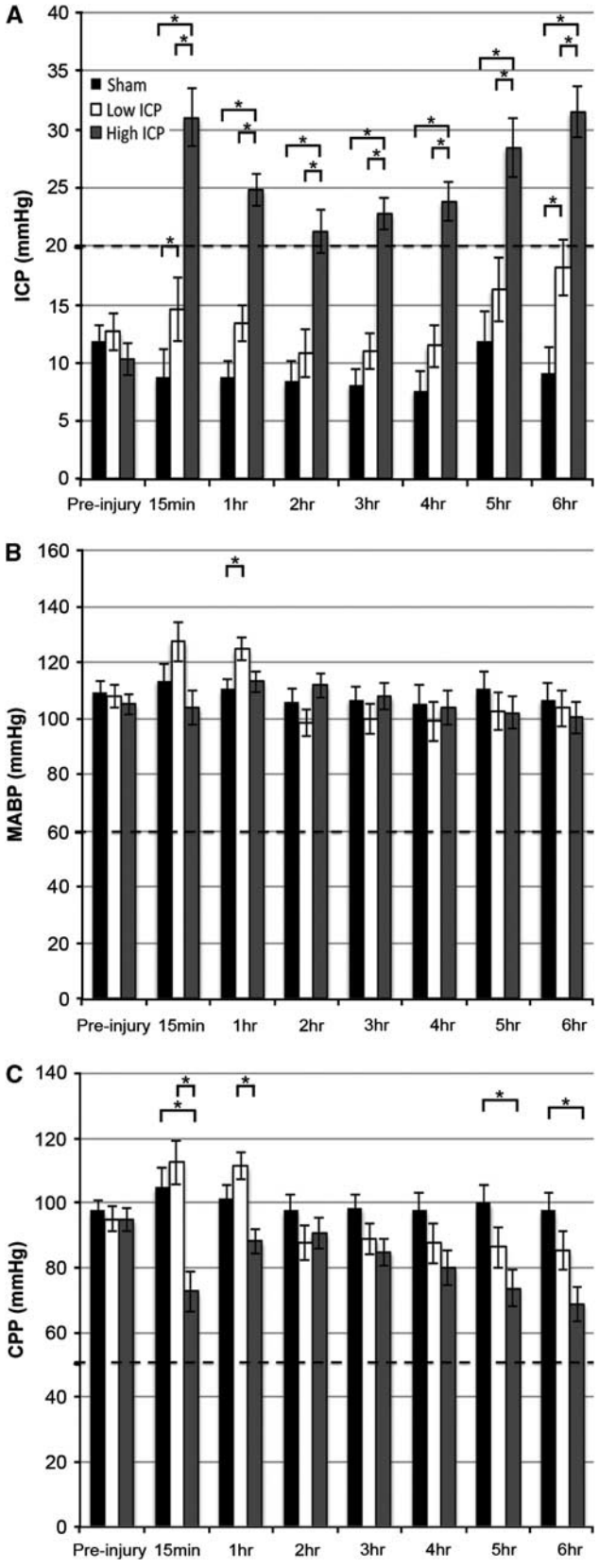

Figure 1 There are two distinct patterns of intracranial pressure (ICP) elevation after injury without resulting in a shift of cerebral perfusion pressure (CPP) below deleterious limits. Upon injury, half of the animals revealed a transient increase in ICP that returned to baseline levels acutely (low ICP group; ICP < 20 mm Hg $\geqslant 65\%$ of the 6 hours after injury analysis) while the other half of the injured animals maintained a consistently elevated ICP (high ICP group; ICP > 20 mm Hg $\geqslant 65\%$ of the 6 hours after injury analysis). A dashed line indicates the 20 mm Hg distinction. Bar graphs representing the mean (**A**) ICP, (**B**) mean arterial blood pressure (MABP), and (**C**) CPP over the time periods indicated of animals in the sham (black), low ICP (white), and high ICP group (dark gray), before and for 6 hours after injury. At no time over the length of the experiment did any group of animals decrease below the accepted autoregulatory limits (MABP < 60 mm Hg and CPP < 50 mm Hg; dashed lines in **B** and **C**). $^*P < 0.05$.

Chronic Neuronal Membrane Perturbation Is Exacerbated by Persistent Injury-Induced Intracranial Pressure Elevation

To further explore the population shift of membrane porated neurons away from resealing and toward delayed opening, an analysis of the percentage of total neurons that sustained mechanoporation either acutely after injury or at a more chronic time after injury was performed. To this end, the number of NeuN+ neurons that contained either the preinjury or postinjury administered dextran was quantified and normalized to the total number of NeuN+ neurons.

In accordance with our previous observations (Singleton and Povlishock, 2004; Farkas *et al*, 2006), sham-injured animals showed interstitial and perivascular dextran diffusion with negligible tracer flooding of either the preinjury or postinjury administered

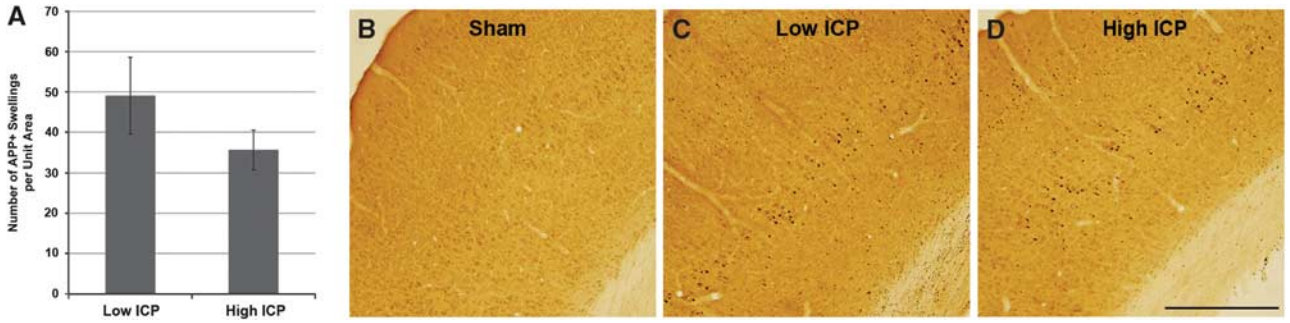

Figure 2 Diffuse axonal transport disruption, indicative of axonal injury, in lateral neocortical layers V and VI was unaltered by the pattern of postinjury intracranial pressure (ICP). (**A**) Bar graph depicting the average number of amyloid precursor protein (APP) immunoreactive axonal swellings in layers V and VI of the lateral neocortex of animals showing high or low ICP after injury. Representative photomicrographs of APP immunoreactivity from (**B**) sham-injured animals and animals with (**C**) low ICP and (**D**) high ICP after injury. Note the absence of APP immunoreactive axonal swellings in the sham-injured controls while the number of swellings is comparable between animals with high versus low ICP after injury. Scale bar: 1 mm.

dextrans (preinjury flooded neurons = 2.16 ± 2.46%; postinjury flooded neurons = 3.22 ± 1.02% per total NeuN+ neurons; Figure 4). However, injured animals revealed neuronal dextran uptake, indicative of membrane perturbation, scattered bilaterally throughout the rostral-caudal extent of the lateral neocortex, primarily within layers V and VI. Virtually, all membrane-perturbed cells were NeuN+ confirming that plasmalemmal disruption is primarily a neuronal pathology *in vivo*.

Elevation of ICP after injury did not affect the percentage of neurons flooded with the preinjury administered dextran (low ICP = 23.76 ± 2.76%; high ICP = 27.19 ± 6.56% per total NeuN+ neurons); however, the percentage of neurons flooded with the postinjury infused dextran doubled with persistently high ICP after injury (low ICP = 18.07 ± 5.14%; high ICP = 38.07 ± 5.49% per total NeuN+ neurons; $P < 0.05$). These findings indicate that the population shift away from resealing toward delayed opening in the high ICP group is due to an increase in neurons that elude acute membrane disruption only to suffer plasmalemmal dysfunction at later time points after injury.

Evidence of Concomitant Neuronal Pathology Without Overt DNA Damage in Neurons Sustaining Chronic Membrane Disruption after Injury

To determine whether elevated ICP was associated with neuronal damage/death at 6 hours after CFPI, an analysis using H&E staining was undertaken. This analysis revealed neurons exhibiting heterochromatic nuclei or eosinophilic cytoplasm, consistent with neuronal damage, in layers V and VI of the lateral neocortex in all three groups, with significantly more damaged neurons identified in animals exhibiting persistently elevated ICP after injury (sham = 5.61 ± 1.44%, $n = 5$; low ICP = 5.97 ± 1.71%, $n = 5$; high ICP = 12.12 ± 1.29% per total neurons, $n = 6$; $P < 0.05$ high ICP versus sham or low ICP; Figure 5J). Neurons showing eosinophilic cytoplasm within the sham-injured population appeared morphologically undamaged and only isolated neurons showed both eosinophilic cytoplasm and heterochromatic nuclei (Figure 5G), whereas the neurons identified as damaged in animals sustaining CFPI appeared pyknotic and showed both eosinophilic cytoplasm and heterochromatic nuclei (Figures 5H and 5I).

To determine whether elevated ICP induced DNA fragmentation associated with more advanced stages of cell death, terminal deoxynucleotidyl transferase-mediated 2′-deoxyuridine 5′-triphosphate-biotin nick end labeling (TUNEL) labeling was conducted using a DNAse-treated section of adult rat brain as a positive control. There were no TUNEL+ cells identified in sham-injured animals and very few TUNEL+ cells in animals sustaining CFPI regardless of postinjury ICP (low ICP = 0.28 ± 0.28%; high ICP = 0.58 ± 0.44% per total Dapi-labeled nuclei; Figure 5E). In agreement with this finding, activated caspase-3 labeling showed no difference between sham and injured animals with either high or low ICP after injury (data not shown).

To further assess the potential for neuronal perturbation and death in this population, concomitant ultrastructural analysis of chronically membrane porated neurons, as identified by immunoelectron microscopy against the postinjury administered dextran (Farkas *et al*, 2006), was performed. The majority of neurons showing cytoplasmic uptake of the postinjury infused dextran without contemporaneous nuclear influx showed little pathological damage (Figure 6A). A subset of chronically membrane porated neurons that showed both cytoplasmic and nuclear uptake of the postinjury infused dextran also showed no overt ultrastructural alteration while others exhibiting the same cytoplasmic and nuclear uptake appeared damaged with evidence of necrotic change. Such necrotic change was reflected in occasional vesicular swelling and increased nuclear and cytoplasmic electron density (Figures 6C and 6D).

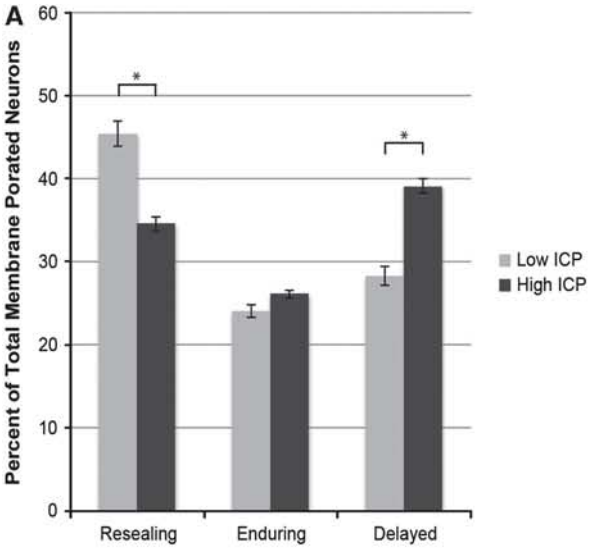

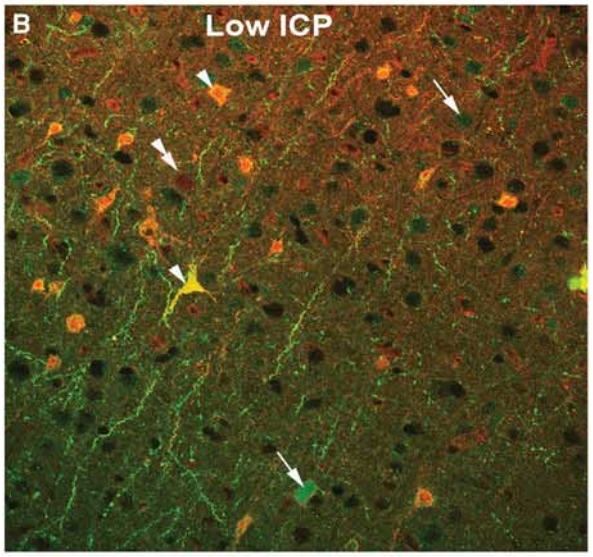

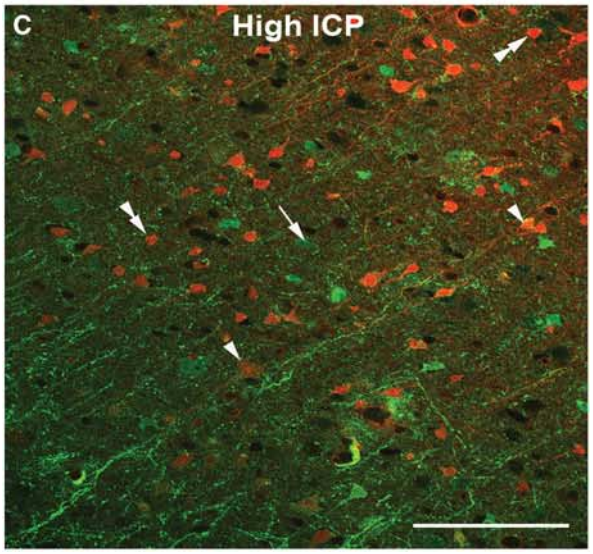

The most severely damaged neurons were comprised predominantly of the population exhibiting enduring mechanoporation and these neurons showed pyknosis, extreme vesicular swelling, mitochondrial alterations, and a redistribution of the lysosomal cysteine protease cathepsin-B from the lysosomal compartment into the cytosol surrounding ruptured lysosomes (Figures 6E and 6F).

Due to the observed redistribution of cathepsin-B in ultrastructurally damaged, chronically membrane porated neurons, the localization of cathepsin-B within the various porated neuronal populations was analyzed ($n = 1{,}419$ total neurons analyzed; $n = 701$ nonmechanoporated neurons; $n = 212$ resealing neurons; $n = 359$ enduring membrane porated neurons; $n = 147$ delayed opening neurons). A shift in the localization of cathepsin-B was noted in neurons sustaining membrane perturbation after injury, with a striking localization shift in neurons sustaining poration at more chronic time points (Figure 7A). Most of the neurons that did not sustain any membrane poration ($89.44 \pm 1.16\%$), as discerned by exclusion of either dextran, showed punctate localization of cathepsin-B indicative of restriction to the lysosomal compartment (Figure 7D). Although fewer neurons that underwent membrane resealing had cathepsin-B localized into puncta ($61.79 \pm 3.34\%$; $P < 0.05$) compared with nonmechanoporated neurons, the majority of resealing neurons showed this phenotype. Unlike nonmechanoporated neurons or neurons with resealed membranes, less than half of the neurons sustaining membrane poration at a more chronic time point postinjury, either with enduring or with delayed membrane perturbation, showed punctate localization of cathepsin-B (enduring = $37.04 \pm 2.55\%$; delayed = $30.61 \pm 3.81\%$; $P < 0.05$ compared with nonmechanoporated or resealing). Rather, chronically membrane porated neurons showed diffusely localized cathepsin-B, indicative of redistribution from lysosomes into the cytosol (Figure 7E). The shift in cathepsin-B localization within the chronically membrane porated population of neurons was observed regardless of postinjury ICP, however, as mentioned previously, animals sustaining high ICP after injury exhibited more chronically porated neurons.

Figure 3 The population of mechanoporated neurons shifts away from a resealing phenotype and toward the delayed opening phenotype with persistently elevated intracranial pressure (ICP) after injury. (**A**) Bar graph depicting the shift from resealing to delayed mechanoporated neurons in animals in the high ICP group (dark gray) as compared with those in the low ICP group (light gray). Representative photomicrographs from dextran-infused animals with (**B**) low ICP and (**C**) high ICP after injury. Note the population shift away from resealing (arrows) and toward delayed (double arrow heads) mechanoporated neurons in the high ICP group, while the enduring (arrow heads) membrane porated neurons remain comparable to the low ICP condition. $^*P < 0.05$. Scale bar: 100 μm.

Discussion

The current study shows the detrimental effects of injury-induced sustained ICP elevation >20 mm Hg on the complex pathobiology after TBI. While the majority of research investigating elevated ICP after TBI has focused exclusively on attendant ischemic pathology precipitated by a drastic reduction in CPP with elevated ICP (Marin-Caballos *et al*, 2005; Li *et al*, 2010), this study is the first report of post-traumatic ICP-associated pathology generated without concurrent reduction of CPP to levels classically associated with cerebral ischemia (Dennis *et al*, 2009; Navarro *et al*, 2012). The absence of homogeneous tissue damage in the neocortex (Bramlett and Dietrich, 2004) coupled with the observation that that fluid percussion injury does not reduce cerebral blood flow to ischemic levels (Yamakami and McIntosh, 1991) also argues against the possibility of ischemic events. Further, the rigorous physiological inclusion criteria implemented in the current study reduce the possibility of introducing variability due to ensuing ischemia.

Our model achieves two naturally occurring injury-induced patterns of ICP, one in which ICP increased >20 mm Hg returning to baseline levels acutely and a second pattern that maintained persistently elevated ICP >20 mm Hg. The group sustaining persistently elevated ICP postinjury may show this phenotype due to blockage of the CSF drainage pathway through the cribriform plate by TBI-induced meningeal bleeding, given that ICP elevation has been linked to blockage of the cribriform plate in noninjured animals (Nagra *et al*, 2006; Mollanji *et al*, 2001). Although, further studies are required to elucidate the exact mechanisms precipitating this ICP phenotype, this model is ideal for the exploration of ICP-associated damaging consequences after diffuse TBI.

This study is also in agreement with previous data reporting that mechanical force associated with traumatic spinal cord or brain injury (Singleton and Povlishock, 2004; Farkas *et al*, 2006; Choo *et al*, 2007; Whalen *et al*, 2008) as well as the induction of mechanical insults *in vitro* (Geddes *et al*, 2003*b*; Kilinc *et al*, 2008; LaPlaca *et al*, 2009; Cullen *et al*, 2011) precipitate plasmalemmal mechanoporation visualized using cell impermeable dyes. This membrane poration can be initiated at the onset of injury and precipitated at more chronic time points after

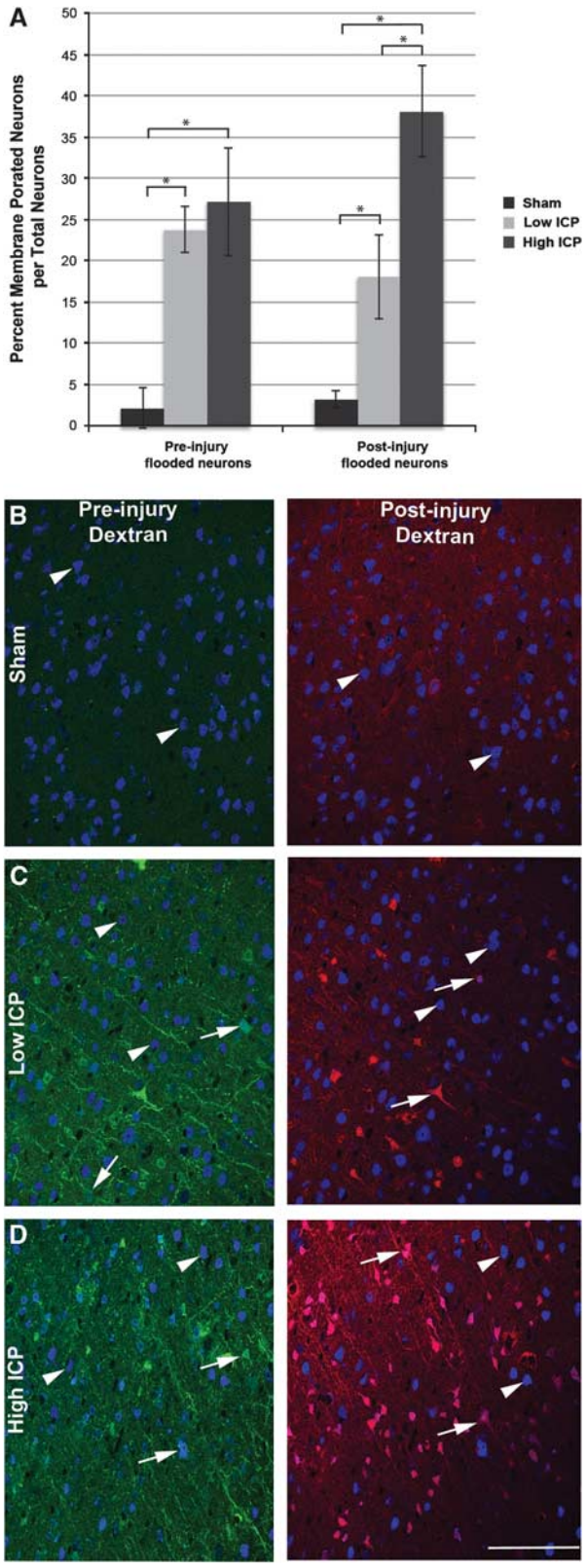

Figure 4 Injury-induced persistently elevated intracranial pressure (ICP) exacerbates chronic neuronal somatic mechanoporation. (**A**) Bar graph depicting the percentage of dextran-flooded NeuN+ neocortical neurons per total neurons analyzed. The high ICP group had double the number of mechanoporated neurons that took up the postinjury infused dextran as compared with the low ICP group, while the number of membrane porated neurons that took up the preinjury infused dextran was analogous. Representative photomicrographs of dextran-infused (preinjury infused dextran: green and postinjury infused dextran: red) animals in the (**B**) sham, (**C**) low ICP, or (**D**) high ICP group labeled with NeuN (blue in **B**–**D**) to identify neurons. Notice the stark contrast between nonmechanoporated (arrow heads) and mechanoporated (arrows) neurons. $*P < 0.05$. Scale bar: 100 μm.

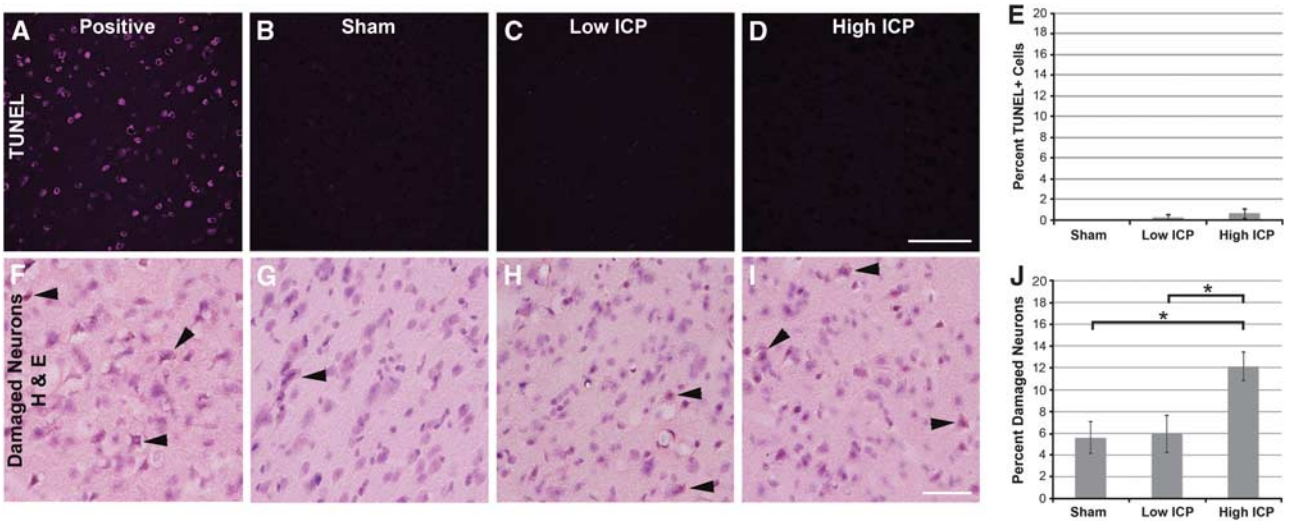

Figure 5 Injury-induced intracranial pressure (ICP) elevation does not precipitate DNA fragmentation but is associated with cell perturbation. Representative photomicrographs from animals sustaining (**B**, **G**) sham injury and animals with either (**C**, **H**) low ICP or (**D**, **I**) high ICP after injury immunolabeled with (**A**–**D**) TUNEL to visualize the number of cells with fragmented DNA, and (**F**–**I**) hematoxylin and eosin (H&E) to visualize damaged neurons (arrows). Corresponding bar graphs depicting the (**E**) percent of total Dapi + cells that were also TUNEL labeled and (**J**) the percent of total neurons that were damaged visualized with H&E within layers V and VI of the lateral neocortex. While there are very few TUNEL-positive cells observed after injury (irrespective of ICP pattern), H&E analysis indicated increased neuronal damage in animals exhibiting persistent ICP elevation after TBI. $*P < 0.05$. Scale bar: 100 μm. TUNEL, terminal deoxynucleotidyl transferase-mediated 2′-deoxyuridine 5′-triphosphate-biotin nick end labeling.

injury (Singleton and Povlishock, 2004; Farkas *et al*, 2006; Cullen *et al*, 2011). Our data show that elevated ICP after TBI affects various neuronal pathologies in different ways. Axonal injury and acute neuronal somatic mechanoporation, both pathological events initiated at the onset of injury, appear unaffected by postinjury ICP. Conversely, membrane poration developing at more chronic times after injury was significantly exacerbated with elevated ICP. These findings highlight the difference between those pathologies that are initiated at the onset of TBI and those that develop more chronically after trauma and their susceptibility to secondary ICP elevation.

Both acute and chronic membrane perturbation have been shown to induce the influx of calcium ions both at the cell soma and at points of cytoskeletal disruption along the neurites (LaPlaca and Thibault, 1998; Geddes *et al*, 2003*b*). The intensity and duration of the mechanical force exerted on the cell is positively correlated to the degree of mechanoporation and the influx of calcium (Lusardi *et al*, 2004*b*). Despite this influx of calcium, mechanoporated neurons have been shown, both within this report and by others, to maintain the potential for repair and membrane resealing (Geddes *et al*, 2003*a*; Farkas *et al*, 2006; Whalen *et al*, 2008; Cullen *et al*, 2011). In the current study, a subset of neurons showing mechanoporation at the initiation of injury underwent membrane resealing, while the neurons that had sustained more chronic membrane poration appear to undergo pathological change that is in agreement with both *in-vitro* and *in-vivo* studies that show a subset of the membrane porated neurons proceeding to cell death (Geddes *et al*, 2003*b*; Lusardi *et al*, 2004*b*). Thus, early ICP management aimed at circumventing the formation of these secondary pathologies could potentially alleviate the ICP-associated negative outcomes described after TBI.

In the current study, the chronically membrane porated cortical neurons do not sustain extensive DNA fragmentation, however, a subset reveal alterations consistent with neuronal perturbation leading to necrotic change. The exacerbation in the percent of damaged neurons associated with elevated postinjury ICP corroborates this finding. The fact that these evaluations were performed at the acute time point of 6 hours, when cell death is not fully unmasked, highlights the importance of early ICP intervention.

Concurrent with the data linking elevated ICP to neuronal damage, other observed neuronal responses also argued for neuronal perturbation; specifically the demonstration that the chronically membrane porated neurons were also found to show a significant redistribution of cathepsin-B compared with those sustaining no mechanoporation or membrane resealing. In a model of spinal cord injury, cathepsin-B was shown upregulated with higher levels of activity at the epicenter of injury 5 days after injury (Ellis *et al*, 2005). The redistribution of cathepsin-B from the lysosomal compartment to the cytosol has previously been observed *in vitro* and after ischemic injury *in vivo* and is associated with an increase in neuronal death and dysfunction (Hill *et al*, 1997; Zhang *et al*, 2009; Kilinc *et al*, 2010; Oberle *et al*, 2010; Wang *et al*, 2011). *In vitro* cathepsin-B has been

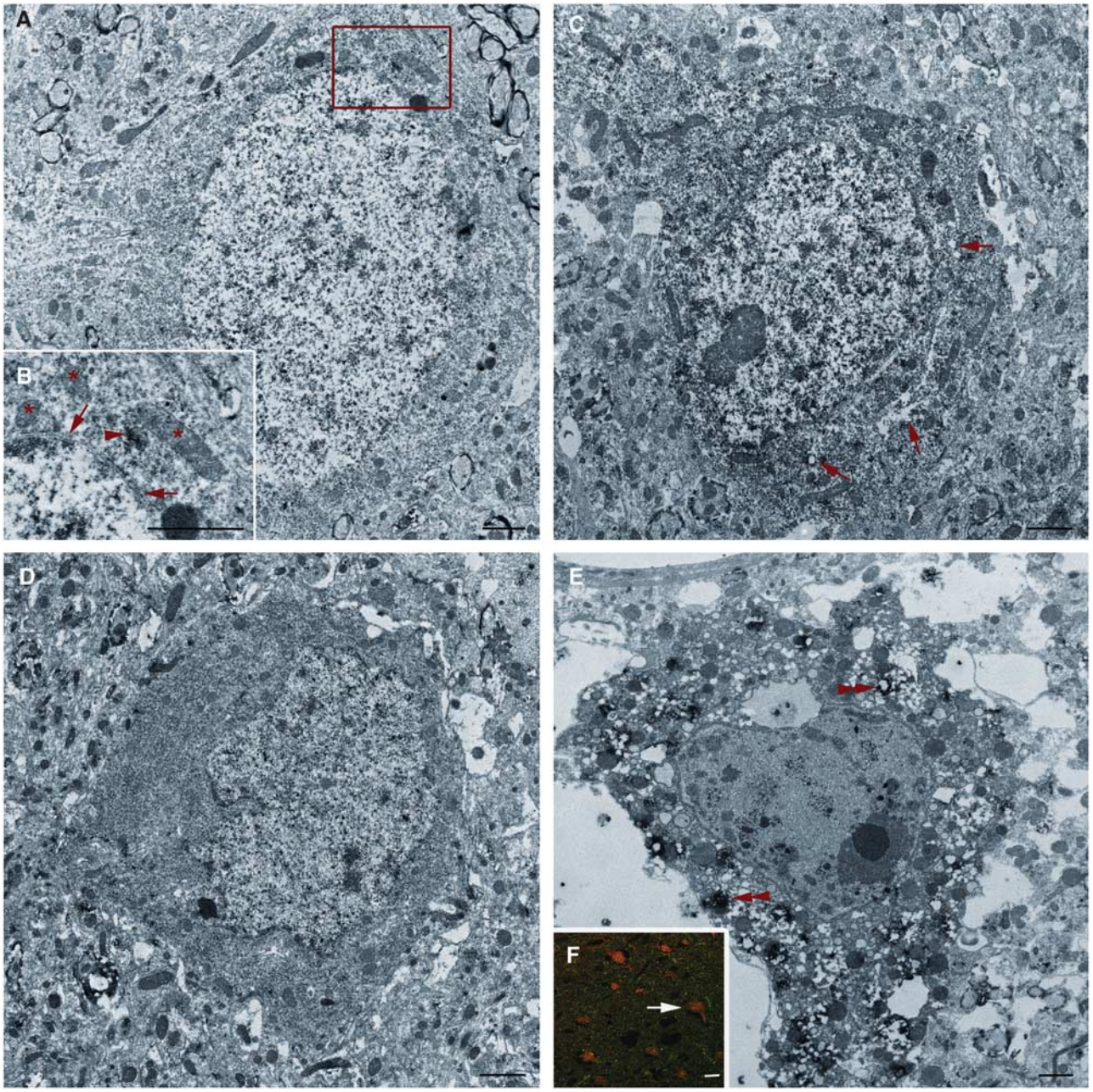

Figure 6 Ultrastructural analysis of chronically mechanoporated neurons revealed morphological heterogeneity. Representative electron micrographs of postinjury infused dextran labeled neurons. (**A**) Many neurons with cytoplasmic dextran incorporation (arrow heads in **B**) without nuclear flooding exhibit intact nuclear membranes (arrows in **B**) and show no overt mitochondrial damage (*), best shown in the enlarged panel (**B**). (**C**) Note that some neurons with both cytoplasmic and nuclear dextran flooding show ultrastructural perturbation including perinuclear organelle vacuolization (arrows in **C**). (**D**) Some neurons containing the postinjury infused dextran also show moderately increased electron density. (**E**) An additional subset of late flooded neurons show overt necrotic change. These neurons undergoing necrotic change, comprised predominantly of the neuronal population exhibiting enduring mechanoporation, as assessed by fluorescent microscopy (arrow in **F** denotes the neuron in **E**) displayed a redistribution of cathepsin-B from the lysosomal compartment into the cytoplasm surrounding what appear to be ruptured lysosomes (double arrow heads). Scale bars: 1 μm **A**–**E**, 10 μm **F**.

shown capable of precipitating cell death under various molecular stimuli within 24 hours when released from lysosomes with compromised membrane integrity in a pathway initiated by cleavage of Bid to form truncated-Bid. Unlike other lysosomal cysteine proteases, such as cathepsin-D, cathepsin-B is fully catalytically active within the cytosol (Pratt *et al*, 2009); therefore, release from the lysosomal compartment can precipitate cytosolic cleavage of Bid. The cleavage of Bid leads to release of AIF and

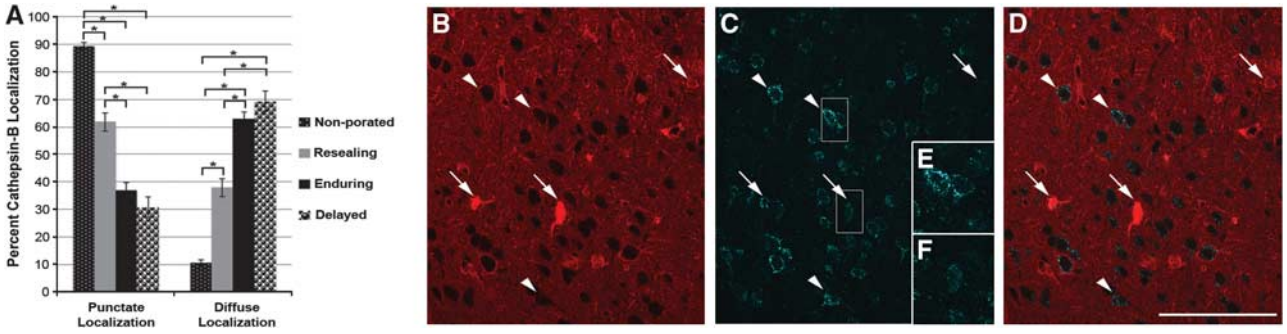

Figure 7 Chronically membrane porated neurons display a redistribution of cathepsin-B. (**A**) Bar graph depicting the percentage of neurons showing punctate (i.e., lysosomal) or diffuse (i.e., cytosolic) localization of cathepsin-B. The majority of neurons exhibiting either no mechanoporation (small white-dotted black bar) or membrane resealing (gray bar) had punctate localization of cathepsin-B, indicative of intact lysosomes. Conversely, the majority of neuron sustaining chronic membrane poration, either enduring (black bar) or delayed opening (large black-dotted white bar), showed diffuse cytoplasmic localization of cathepsin-B, suggestive of lysosomal rupture. Representative confocal photomicrographs of (**B**) the postinjury infused dextran, (**C**) cathepsin-B immunoreactivity of the same region, and (**D**) an overlay showing the redistribution of cathepsin-B from punctate lysosomal compartments, typical of nonmechanoporated neurons (arrow heads), to diffuse cytosolic localization in neurons sustaining chronic membrane poration (arrows). Enlarged photomicrographs of cathepsin-B labeling in (**E**) nonmechanoporated and (**F**) chronically mechanoporated neurons demarcated with white boxes in (**B**). $*P < 0.05$. Scale bar: 100 μm.

cytochrome c from mitochondria, which then activate cell death pathways in a caspase-3-independent manner (Yacoub *et al*, 2006; Zhang *et al*, 2009). The use of cathepsin-B inhibitors has also proved therapeutically relevant in models of ischemia and trauma, reducing lesion size, and improving outcomes after injury (Yoshida *et al*, 2002). Other studies, however, determined that cathepsin-B has a pro-survival function that counteracts cathepsin-D signaling (Nagai *et al*, 2005). These conflicting roles show the complexity of cathepsin-B signaling and will require further investigation to determine the exact role of the redistribution seen in membrane porated neurons.

In summary, this study provides new insight into the secondary pathology associated with diffuse TBI and forces a reevaluation of current dogma surrounding TBI-induced ICP elevation. Elevation of ICP, independent of a correlated reduction in CPP to detrimental levels, is harmful and significantly exacerbates neuronal perturbation even at acute time points after injury. Furthermore, the neurons sustaining chronic membrane poration appear to be associated with the activation of a potentially pathological pathway involving cathepsin-B redistribution and ultimate neuronal perturbation. Conceivably, these damaging sequelae could be circumvented with more aggressive ICP monitoring and management. The above findings speak to the complexity of TBI as well as the potential need for increased vigilance in monitoring and controlling ICP in both animals and humans.

Acknowledgements

The authors thank Dr Scott Henderson for his expertise in microscopy and image analysis, Dr Robert Hamm for statistical expertise, and Sue Walker, C Lynn Davis and Jesse Sims for invaluable technical assistance.

Disclosure/conflict of interest

The authors declare no conflict of interest.

References

Bramlett HM, Dietrich WD (2004) Pathophysiology of cerebral ischemia and brain trauma: similarities and differences. *J Cereb Blood Flow Metab* 24:133–50

Bratton SL, Chestnut RM, Ghajar J, McConnell Hammond FF, Harris OA, Hartl R, Manley GT, Nemecek A, Newell DW, Rosenthal G, Schouten J, Shutter L, Timmons SD, Ullman JS, Videtta W, Wilberger JE, Wright DW (2007*a*) Guidelines for the management of severe traumatic brain injury. IX. Cerebral perfusion thresholds. *J Neurotrauma* 24(Suppl 1):S59–64. (Information also online at https://www.braintrauma.org/coma-guidelines/)

Bratton SL, Chestnut RM, Ghajar J, McConnell Hammond FF, Harris OA, Hartl R, Manley GT, Nemecek A, Newell DW, Rosenthal G, Schouten J, Shutter L, Timmons SD, Ullman JS, Videtta W, Wilberger JE, Wright DW (2007*b*) Guidelines for the management of severe traumatic brain injury. VI. Indications for intracranial pressure monitoring. *J Neurotrauma* 24(Suppl 1):S37–44. (Information also online at https://www.braintrauma.org/coma-guidelines/)

Choo AM, Liu J, Lam CK, Dvorak M, Tetzlaff W, Oxland TR (2007) Contusion, dislocation, and distraction: primary hemorrhage and membrane permeability in distinct mechanisms of spinal cord injury. *J Neurosurg Spine* 6:255–66

Cullen DK, Vernekar VN, LaPlaca MC (2011) Trauma-induced plasmalemma disruptions in three-dimensional neural cultures are dependent on strain modality and rate. *J Neurotrauma* 28:2219–33

Dennis AM, Haselkorn ML, Vagni VA, Garman RH, Janesko-Feldman K, Bayir H, Clark RS, Jenkins LW, Dixon CE, Kochanek PM (2009) Hemorrhagic shock after experimental traumatic brain injury in mice: effect on neuronal death. *J Neurotrauma* 26:889–99

Dixon CE, Lyeth BG, Povlishock JT, Findling RL, Hamm RJ, Marmarou A, Young HF, Hayes RL (1987) A fluid percussion model of experimental brain injury in the rat. *J Neurosurg* 67:110–9

Ellis RC, O'Steen WA, Hayes RL, Nick HS, Wang KK, Anderson DK (2005) Cellular localization and enzymatic activity of cathepsin B after spinal cord injury in the rat. *Exp Neurol* 193:19–28

Farkas O, Lifshitz J, Povlishock JT (2006) Mechanoporation induced by diffuse traumatic brain injury: an irreversible or reversible response to injury? *J Neurosci* 26: 3130–40

Geddes DM, Cargill RS, II, LaPlaca MC (2003*a*) Mechanical stretch to neurons results in a strain rate and magnitude-dependent increase in plasma membrane permeability. *J Neurotrauma* 20:1039–49

Geddes DM, LaPlaca MC, Cargill RS, II (2003*b*) Susceptibility of hippocampal neurons to mechanically induced injury. *Exp Neurol* 184:420–7

Hesdorffer DC, Ghajar J, Iacono L (2002) Predictors of compliance with the evidence-based guidelines for traumatic brain injury care: a survey of United States trauma centers. *J Trauma* 52:1202–9

Hill IE, Preston E, Monette R, MacManus JP (1997) A comparison of cathepsin B processing and distribution during neuronal death in rats following global ischemia or decapitation necrosis. *Brain Res* 751:206–16

Kilinc D, Gallo G, Barbee KA (2008) Mechanically-induced membrane poration causes axonal beading and localized cytoskeletal damage. *Exp Neurol* 212:422–30

Kilinc M, Gursoy-Ozdemir Y, Gurer G, Erdener SE, Erdemli E, Can A, Dalkara T (2010) Lysosomal rupture, necroapoptotic interactions and potential crosstalk between cysteine proteases in neurons shortly after focal ischemia. *Neurobiol Dis* 40:293–302

Langlois JA, Rutland-Brown W, Wald MM (2006) The epidemiology and impact of traumatic brain injury: a brief overview. *J Head Trauma Rehabil* 21:375–8

LaPlaca MC, Prado GR, Cullen D, Simon CM (2009) Plasma membrane damage as a marker of neuronal injury. *Conf Proc IEEE Eng Med Biol Soc* 2009:1113–6

LaPlaca MC, Thibault LE (1998) Dynamic mechanical deformation of neurons triggers an acute calcium response and cell injury involving the N-methyl-D-aspartate glutamate receptor. *J Neurosci Res* 52:220–9

Li LM, Timofeev I, Czosnyka M, Hutchinson PJ (2010) Review article: the surgical approach to the management of increased intracranial pressure after traumatic brain injury. *Anesth Analg* 111:736–48

Lusardi TA, Wolf JA, Putt ME, Smith DH, Meaney DF (2004*b*) Effect of acute calcium influx after mechanical stretch injury *in vitro* on the viability of hippocampal neurons. *J Neurotrauma* 21:61–72

Marin-Caballos AJ, Murillo-Cabezas F, Cayuela-Dominguez A, Dominguez-Roldan JM, Rincon-Ferrari MD, Valencia-Anguita J, Flores-Cordero JM, Munoz-Sanchez MA (2005) Cerebral perfusion pressure and risk of brain hypoxia in severe head injury: a prospective observational study. *Crit Care* 9:R670–6

Miller JD, Becker DP, Ward JD, Sullivan HG, Adams WE, Rosner MJ (1977) Significance of intracranial hypertension in severe head injury. *J Neurosurg* 47:503–16

Mollanji R, Bozanovic-Sosic R, Silver I, Li B, Kim C, Midha R, Johnston M (2001) Intracranial pressure accommodation is impaired by blocking pathways leading to extracranial lymphatics. *Am J Physiol Regul Integr Comp Physiol* 280:R1573–81

Nagai A, Ryu JK, Terashima M, Tanigawa Y, Wakabayashi K, McLarnon JG, Kobayashi S, Masuda J, Kim SU (2005) Neuronal cell death induced by cystatin C *in vivo* and in cultured human CNS neurons is inhibited with cathepsin B. *Brain Res* 1066:120–8

Nagra G, Koh L, Zakharov A, Armstrong D, Johnston M (2006) Quantification of cerebrospinal fluid transport across the cribriform plate into lymphatics in rats. *Am J Physiol Regul Integr Comp Physiol* 291:R1383–9

Navarro JC, Pillai S, Cherian L, Garcia R, Grill RJ, Robertson CS (2012) Histopathological and behavioral effects of immediate and delayed hemorrhagic shock after mild traumatic brain injury in rats. *J Neurotrauma* 29:322–34

Oberle C, Huai J, Reinheckel T, Tacke M, Rassner M, Ekert PG, Buellesbach J, Borner C (2010) Lysosomal membrane permeabilization and cathepsin release is a Bax/Bak-dependent, amplifying event of apoptosis in fibroblasts and monocytes. *Cell Death Differ* 17:1167–78

Pratt MR, Sekedat MD, Chiang KP, Muir TW (2009) Direct measurement of cathepsin B activity in the cytosol of apoptotic cells by an activity-based probe. *Chem Biol* 16:1001–12

Reid WM, Rolfe A, Register D, Levasseur JE, Churn SB, Sun D (2010) Strain-related differences after experimental traumatic brain injury in rats. *J Neurotrauma* 27: 1243–53

Sherriff FE, Bridges LR, Gentleman SM, Sivaloganathan S, Wilson S (1994) Markers of axonal injury in post mortem human brain. *Acta Neuropathol* 88:433–9

Singleton RH, Povlishock JT (2004) Identification and characterization of heterogeneous neuronal injury and death in regions of diffuse brain injury: evidence for multiple independent injury phenotypes. *J Neurosci* 24:3543–53

Stone JR, Singleton RH, Povlishock JT (2000) Antibodies to the C-terminus of the beta-amyloid precursor protein (APP): a site specific marker for the detection of traumatic axonal injury. *Brain Res* 871:288–302

Sullivan HG, Martinez J, Becker DP, Miller JD, Griffith R, Wist AO (1976) Fluid-percussion model of mechanical brain injury in the cat. *J Neurosurg* 45:521–34

Treggiari MM, Schutz N, Yanez ND, Romand JA (2007) Role of intracranial pressure values and patterns in predicting outcome in traumatic brain injury: a systematic review. *Neurocrit Care* 6:104–12

Wang JY, Xia Q, Chu KT, Pan J, Sun LN, Zeng B, Zhu YJ, Wang Q, Wang K, Luo BY (2011) Severe global cerebral ischemia-induced programmed necrosis of hippocampal CA1 neurons in rat is prevented by 3-methyladenine: a widely used inhibitor of autophagy. *J Neuropathol Exp Neurol* 70:314–22

Whalen MJ, Dalkara T, You Z, Qiu J, Bermpohl D, Mehta N, Suter B, Bhide PG, Lo EH, Ericsson M, Moskowitz MA (2008) Acute plasmalemma permeability and protracted clearance of injured cells after controlled cortical impact in mice. *J Cereb Blood Flow Metab* 28:490–505

Yacoub A, Park MA, Hanna D, Hong Y, Mitchell C, Pandya AP, Harada H, Powis G, Chen CS, Koumenis C, Grant S, Dent P (2006) OSU-03012 promotes caspase-independent but PERK-, cathepsin B-, BID-, and AIF-dependent killing of transformed cells. *Mol Pharmacol* 70:589–603

Yamakami I, McIntosh TK (1991) Alterations in regional cerebral blood flow following brain injury in the rat. *J Cereb Blood Flow Metab* 11:655–60

Yoshida M, Yamashima T, Zhao L, Tsuchiya K, Kohda Y, Tonchev AB, Matsuda M, Kominami E (2002) Primate neurons show different vulnerability to transient ischemia and response to cathepsin inhibition. *Acta Neuropathol* 104:267–72

Zhang H, Zhong C, Shi L, Guo Y, Fan Z (2009) Granulysin induces cathepsin B release from lysosomes of target tumor cells to attack mitochondria through processing of bid leading to Necroptosis. *J Immunol* 182:6993–7000